CityU Scholars

Ultralow-loss fusion splicing between negative curvature hollow-core fibers and conventional SMFs with a reverse-tapering method

WANG, Caoyuan; YU, Ruowei; DEBORD, Benoît; GÉRÔME, Frédéric; BENABID, Fetah; CHIANG, Kin Seng; XIAO, Limin

Document Version:
Final Published version, also known as Publisher's PDF, Publisher's Final version or Version of Record

Publication record in CityU Scholars:
Go to record

Ultralow-loss fusion splicing between negative curvature hollow-core fibers and conventional SMFs with a reverse-tapering method

Caoyuan Wang,[1,4] Ruowei Yu,[1,4] Benoît Debord,[2] Frédéric Gérôme,[2] Fetah Benabid,[2] Kin Seng Chiang,[3] [iD] and Limin Xiao[1,5] [iD]

[1]*Advanced Fiber Devices and Systems Group, Key Laboratory of Micro and Nano Photonic Structures (MoE), Key Laboratory for Information Science of Electromagnetic Waves (MoE), Shanghai Engineering Research Center of Ultra-Precision Optical Manufacturing, School of Information Science and Technology, Fudan University, Shanghai 200433, China*

[2]*GPPMM group, XLIM Research Institute, CNRS UMR 7252, Université de Limoges, Limoges 87032, France*

[3]*Department of Electrical Engineering, City University of Hong Kong, 83 Tat Chee Avenue, Kowloon, Hong Kong SAR, China*

[4]*These authors contributed equally to this work*

[5]*liminxiao@fudan.edu.cn*

Abstract: Negative curvature hollow-core fibers (NC-HCFs) can boost the excellent performance of HCFs in terms of propagation loss, nonlinearity, and latency, while retaining large core and delicate cladding structures, which makes them distinctly different from conventional fibers. Construction of low-loss all-fiber NC-HCF architecture with conventional single-mode fibers (SMFs) is important for various applications. Here we demonstrate an efficient and reliable fusion splicing method to achieve low-loss connection between a NC-HCF and a conventional SMF. By controlling the mode-field profile of the SMF with a two-step reverse-tapering method, we realize a record-low insertion loss of 0.88 dB for a SMF/NC-HCF/SMF chain at 1310 nm. Our method is simple, effective, and reliable, compared with those methods that rely on intermediate bridging elements, such as graded-index fibers, and can greatly facilitate the integration of NC-HCFs and promote more advanced applications with such fibers.

1. Introduction

A hollow-core fiber (HCF), an optical fiber with a hollow core surrounded by a microstructured cladding, exhibits the ability to guide light in air, which enables a wide range of new applications [1–12]. Among these HCFs, the negative curvature HCF (NC-HCF), also called the tubular-lattice hollow-core photonic crystal fiber, has attracted intensive attention in recent years, which possesses an isolated tubular lattice cladding and guides light in the hollow core owing to the mechanism of inhibited-coupling whereby the interaction between cladding modes and core mode is strongly suppressed [2]. Due to its unique properties of ultralow propagation loss [3], broad transmission window [1,2], ultralow nonlinearity [4], low latency [5], and low thermal sensitivity [6], NC-HCF has the potential to serve as a powerful photonic platform for applications in advanced optical telecommunication [5], sensing [7,8], and high-power laser generation and delivery [9–11], etc. Despite these advantages, the inherent large core size of NC-HCFs (30 μm or even larger) [1–12], results in a considerable mode-field mismatch and large coupling loss with conventional single-mode fibers (SMFs), which seriously limits efficient integration of NC-HCFs with the existing fiber devices and systems.

Several attempts and progress have been made to improve the butt-coupling or splicing efficiency between a NC-HCF and a SMF [5,13–22]. For example, W. Huang *et al*. have achieved a butt-coupling loss of 0.77 dB [13] measured from the SMF to the NC-HCF by using a tapered SMF and H. Li et al. have achieved a total insertion loss of 2.81 dB for double end coupling [14]. However, a tapered SMF cannot be spliced to a NC-HCF, causes difficulties in packaging and raises mechanical robustness issues. X. Zheng et al. [15] have demonstrated that a NC-HCF can be precisely tapered without destroying its delicate core-contour negative curvature, and they have achieved a splicing loss of 0.48 dB measured from the SMF to the NC-HCF and a reverse splicing loss of 3.5 dB at 1550 nm. In these two methods, the reverse coupling losses are much larger, because the high-order modes excited in the NC-HCF create large coupling losses to the SMF. It is, in fact, a challenge to excite only the fundamental mode of the NC-HCF and achieve low coupling losses in both directions. Another butt-coupling method based on the use of a silica ball [16] has also been demonstrated, but the coupling loss measured from the NC-HCF to the SMF was still high up to 3 dB. To improve mode-field match and minimize high-order mode excitation, a graded-index (GRIN) fiber has recently been used as a mode-field adapter to bridge between the SMF and the NC-HCF [18–20]. By using a bridging fiber, the butt-coupling loss achieved for a SMF/NC-HCF/SMF chain is 1 dB, where antireflective coatings are applied to the fiber interfaces [19]. Recently, the butt-coupling loss of the chain has been improved to a record-low value of 0.3 dB [20]. However, it is difficult to splice fibers with coated tips, as the coating can be destroyed in the high-temperature fusion process. Using GRIN bridging fibers without antireflective coatings, the splice losses of the chain are in the range of 1.25–3.7 dB [5,21,22], which represent the lowest fusion splicing losses of the chain reported so far. A disadvantage of that method is that the length of the GRIN bridging fiber must be controlled to within several to tens of micrometers [18–20], which can be a serious issue for achieving good repeatability in the splicing process. It remains a challenge to develop a highly repeatable fusion splicing process for the construction of low-loss all-fiber NC-HCF links.

In this paper, we report a record-low fusion splicing total loss of 0.88 dB for a SMF/NC-HCF/SMF chain without using any intermediate bridging fibers. The average splicing loss of each joint in the chain is ~0.44 dB in the wavelength range from 1150 nm to 1500 nm, except at the OH$^-$ absorption peak near 1383 nm. Our splicing method is based on two-step reverse tapering [23], where the mode-field diameter (MFD) and the mode profile of the SMF are precisely controlled to match those of the NC-HCF. Compared with the method of using a GRIN bridging fiber, our method is simpler and more cost-effective, and can improve not only the splicing efficiency but also the repeatability. In addition, our method can reduce the cladding size mismatch of the two fibers and thus significantly increase the splicing strength.

2. Method and analysis

The NC-HCF used in our study is from GPPMM group, XLIM Research Institute, as shown in Fig. 1(a). It is characterized by a negative-curvature hollow core and a single-ring isolated tubular lattice cladding. The diameters of the core, the inner cladding, and the outer cladding are 30 μm, 51 μm, and 200 μm, respectively. There are eight tubes in the inner cladding and Fig. 1(b) shows a scanning electron micrograph (SEM) of one tube. Each tube has a diameter of 10.7 μm and a thickness as low as ~340 nm, and the average gap between two adjacent tubes is 4.75 μm. Figure 1(c) shows the measured mode pattern in the NC-HCF at the wavelength 830 nm, exhibiting tight single-mode confinement in the hollow core. The NC-HCF has a propagation loss smaller than 0.3 dB/m in the broad spectral range from ~700 nm to ~1500 nm, as shown in Fig. 1(d). Specifically, at 1310 nm, the transmission loss is 0.16 dB/m and the MFD is 25.2 μm.

The SMF used is the conventional SMF-28 from Corning, which has a core diameter of 8.2 μm, a cladding diameter of 125 μm, and a MFD of 9.2 μm at 1310 nm. The cutoff wavelength of SMF-28 is ~1260 nm. The theoretical fundamental mode mismatch loss between SMF-28
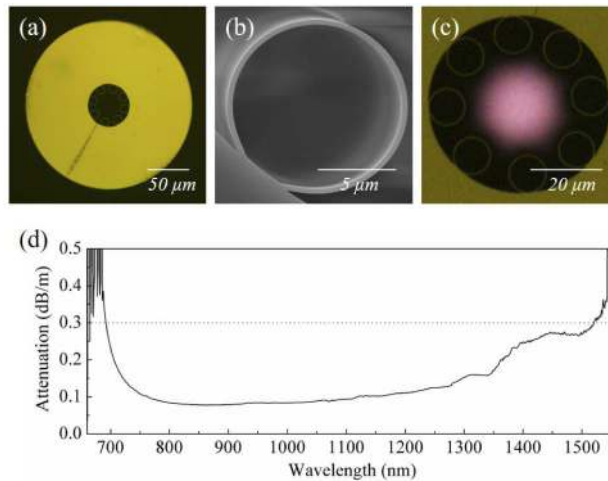
Fig. 1. (a) Microscopic image of the NC-HCF; (b) a magnified SEM image of a tube in the tubular lattice structure of the NC-HCF; (c) measured mode pattern in the NC-HCF at the wavelength 830 nm; and (d) measured attenuation spectrum of the NC-HCF.

and the NC-HCF calculated by the fiber mode coupling theory [24] is ∼3.2 dB at 1310 nm. We performed direct fusion splicing between the two fibers and obtained an average splicing loss of 2.86 dB measured from the SMF to the NC-HCF. The fact that the experimental coupling loss is smaller than the theoretical value indicates that part of the power coupled to the high-order modes of the NC-HCF is detected. As a large-core HCF supports high-order modes, the coupling loss measured from a SMF to a large-core HCF is usually smaller than that measured from the reverse direction [14,15,25]. Another challenge in the splicing between a SMF and a NC-HCF is the weak strength of the fusion joint. To preserve the delicate structure of the NC-HCF at the joint, a relatively low fusion power (the "cold" splicing method) [26] is generally used to minimize the deformation of the fiber, which, however, can significantly reduce the strength of the joint. The presence of the stress concentration effect at the joint, which arises from the large difference in the cladding diameters of the two fibers, can further weaken the strength of the joint [27]. The joint from direct splicing of SMF-28 to the NC-HCF can only bear a tension load of 52 g. The main challenge in fusion splicing between the SMF and the NC-HCF is to achieve matching of both the overall sizes and the mode-field distributions of the two fibers.

Recently, we have achieved low-loss splicing between a solid-core ultra-large-mode-area photonic-crystal fiber (ULMA-PCF) and a conventional SMF with a two-step reverse-tapering method [23], where the mode-field distribution and the cladding size of the SMF can be precisely controlled to achieve optimal matching with the solid-core ULMA-PCF. Since the NC-HCF is also a large-mode-area fiber, it should be possible, in principle, to splice the NC-HCF and the SMF together with this two-step reverse-tapering method. However, the NC-HCF has a hollow core with a nano-membrane tubular cladding structure and a core size even larger than that of the solid-core ULMA-PCF [23]. To apply the two-step reverse-tapering process to the NC-HCF, it is necessary to perform an even larger reverse mode size transformation of the SMF. Specifically, the mode area of SMF-28 must be adiabatically enlarged by ∼7 times from 66 μm^2 to ∼500 μm^2 with a low loss, and its mode-field distribution should also be controlled to match that of the NC-HCF at the splicing interface.

The strategy of our method is described as follows. First, SMF-28 is reversely tapered at a tapering ratio of two, which doubles the sizes of the core and the cladding to 16.4 μm and 250 μm, respectively. The MFD of the reverse tapered SMF is increased to 13.4 μm at 1310 nm, as shown

in the initial point of Fig. 2(a). Second, the MFD of the reverse taper is further expanded by the thermally expanded core (TEC) process [28] without changing much the normalized frequency of the fiber. The side view in Fig. 2(a) shows the matching of the reversely tapered fiber with the NC-HCF. The important point is that the mode-field distribution of the TEC-treated reversely tapered SMF is closer to that of the NC-HCF, compared with that of the TEC-treated 125-μm SMF. We calculate the coupling loss from SMF-28 to the NC-HCF as a function of the MFD of the reversely tapered SMF under TEC treatment. The results are shown in Fig. 2(a). With an increase in the TEC duration, the MFD of the SMF increases, and the mode-field distribution is modified. When the mode fields of the two fibers are optimally matched (Taper 1), the MFD of the SMF is 21.6 μm and that of the NC-HCF is 24.4 μm, which gives a minimum coupling loss of 0.25 dB. This loss is limited by the Fresnel reflection (~0.15 dB) and the imperfect mode-profile matching at the joint. By using a longer TEC duration, the MFDs of the SMF and the NC-HCF can be made equal (Taper 2). We should note that the minimal coupling loss is not achieved when the MFDs of the two fibers are equal, which is consistent with the previous studies of bandgap HCF coupling [24,29], where the minimum coupling loss is achieved with slightly different MFDs. As shown in Fig. 2(b), the mode profiles of the NC-HCF and the TEC-treated SMF tapers are not perfect Gaussian functions. The intensity distribution of Taper 2 in the tail part is actually slightly larger than that of the NC-HCF, regardless of their equal MFDs, which results in a slightly larger coupling loss. Nevertheless, for both Taper 1 and Taper 2, the theoretical coupling losses are smaller than 0.35 dB. The insets in Fig. 2(a) show the simulated mode patterns of the SMF, the optimally tapered SMF at the joint interface (Taper 1), and the NC-HCF, respectively.
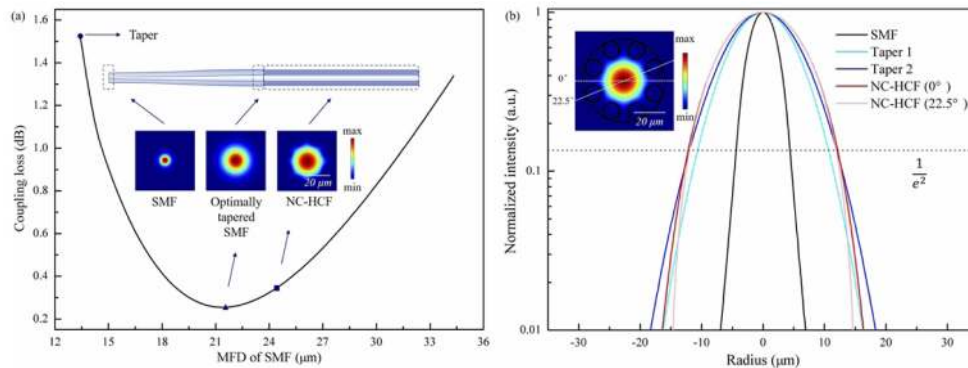
Fig. 2. (a) Calculated coupling loss between the SMF and the NC-HCF as a function of the MFD of the reversely tapered SMF under TEC treatment (MFD is defined as the radial position where the mode intensity falls to e^{-2} of the peak value), where the insets show the coupling between a reversely tapered SMF and the NC-HCF and simulated mode patterns of the SMF, the optimally tapered SMF (Taper 1) at the joint interface, and the NC-HCF on the same scale; and (b) mode profiles of the SMF, two reverse tapers of SMF (Taper 1 and Taper 2), and the NC-HCF, where the inset shows the mode pattern of the NC-HCF.

3.   Experimental results and discussion

To implement the two-step reverse-tapering process on the SMF, a home-made tapering rig was used [23]. A bare SMF section bathed in an oxy-hydrogen flame was compressed from both sides of the rig to form a fattened waist and two bridging transitions. The diameters of the cladding and the core were enlarged at the same ratio by controlling the tapering conditions, namely the temperature, the sweep parameters of the flame, and the pushing parameters of fiber. Special care was taken to avoid bending of the fiber when the fiber was pushed inward from the two sides.

The TEC process was implemented by heating the fiber with a brushed flame, which caused thermal dopant diffusion in the fiber. By controlling the heating temperature and the heating duration, the core diameter and the MFD were further increased to the desired values. By using a reverse-tapering duration of 70 seconds and a TEC duration of 7 minutes, we obtained, at the waist of the reverse taper, a cladding diameter of 250 μm and a MFD of 25.0 μm. We should note that the TEC duration used in the present experiments is much longer than that used in our previous work [23], because of the need to produce a larger MFD. As a result, the total loss induced by the tapering/TEC process in the present case is slightly larger than that reported in [23], but is still smaller than 0.1 dB (measured at 1310 nm).

We next characterized the reverse tapers and their mode properties. Figures 3(a) and 3(b) are side-view images showing the initial untreated 125-μm SMF and the reversely tapered SMF with a cladding diameter of 250 μm. The SMF taper has a transition length of ∼6 mm and a waist length of ∼0.5 mm. These results confirm the ability of controlling the fiber size by reverse tapering of the fiber. To produce the optimized reverse tapers, Taper 1 and Taper 2, TEC durations of 6.75 minutes and 7.0 minutes were used, respectively. Figure 3(c) shows the measured normalized near-field intensity profiles (at 1310 nm) of the 125-μm SMF, Taper 1, Taper 2, and the NC-HCF, which were captured by an infrared camera (Xeva XC-130). The MFDs of these fibers are 10.3 μm, 21.6 μm, 25.2 μm, and 25.0 μm, respectively. The mode-profiles of the tapers shown in Fig. 3(c) confirm good matching with the NC-HCF. These results fully demonstrate our ability of controlling the mode size and the mode profile of the SMF.
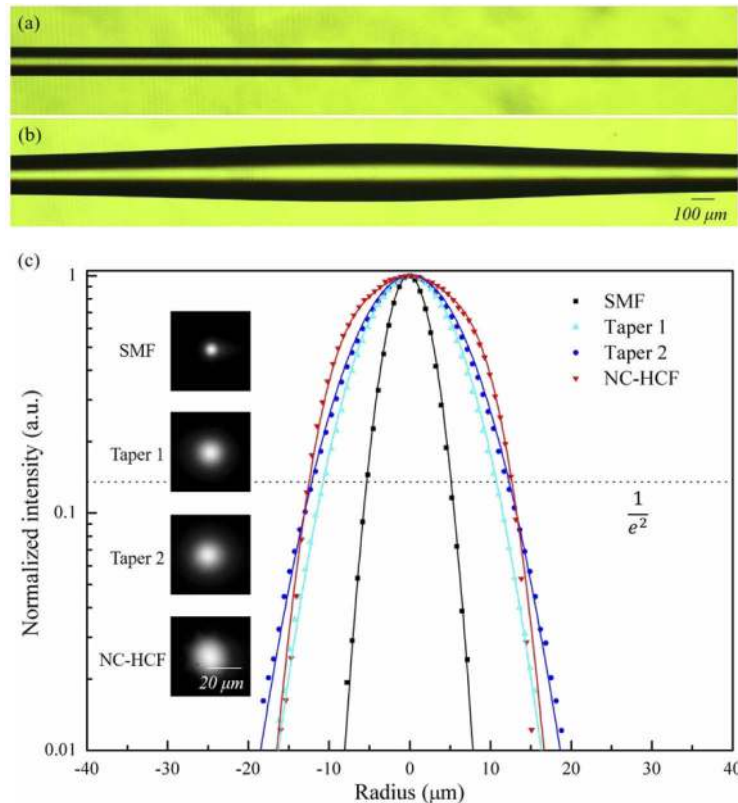
Fig. 3. Side-view images showing (a) the initial SMF with a cladding diameter of 125 μm and (b) the reversely tapered SMF with a cladding diameter of 250 μm at its waist; and (c) measured normalized intensity profiles of the 125-μm SMF, Taper 1, Taper 2, and the NC-HCF.

We investigated the repeatability of the reverse-tapering process with eight taper samples divided into two groups. All the tapers had the same cladding diameter of 250 μm. Four tapers were TEC-treated as for Taper 1 and the other four were TEC-treated as for Taper 2. Figures 4(a) and 4(b) show the near-field intensity profiles and output patterns measured at the waists of the Taper 1 group tapers and the Taper 2 group tapers, respectively. For the Taper 1 group, as shown in Fig. 4(a), the MFDs of the four tapers are 21.56 μm, 21.13 μm, 21.31 μm, and 21.34 μm, respectively. The average and the standard deviation of the MFDs are 21.34 μm and 0.15 μm (i.e., 0.7% of relative deviation), respectively. For the Taper 2 group, as shown in Fig. 4(b), the MFDs of the four tapers are 24.99 μm, 24.64 μm, 24.97 μm, and 24.39 μm, respectively. The average and the standard deviation of the MFDs are 24.75 μm and 0.25 μm (i.e., 1% of relative deviation), respectively. Our measurement results confirm excellent repeatability of our taper fabrication process. We should note that the mode-field distribution and the MFD of the SMF reverse taper is insensitive to the cleaving position along the waist of the taper.
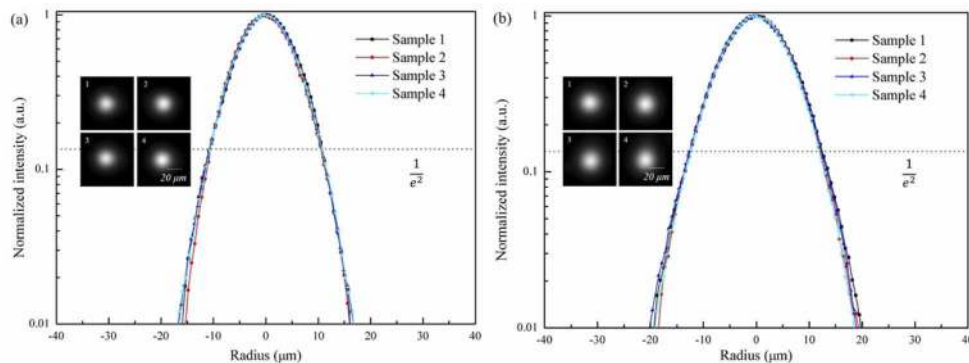
Fig. 4. Near-field intensity profiles and output patterns measured at 1310 nm for (a) the Taper 1 group tapers and (b) the Taper 2 group tapers.

The splicing between a SMF reverse taper and the NC-HCF was performed with a commercial splicing system (Vytran GPX3400). The SMF taper was first cleaved at its waist to an end-face angle smaller than 0.2° with a tension-scribe cleaver (Fujikura CT-100) set at a tension of 670 g. The cleaved taper was then spliced to the NC-HCF. Care was taken to avoid the destruction of the cladding structure of the NC-HCF during splicing. In our experiments, a graphite filament was used and, after some trials, the filament power, the fusion time, and the longitudinal fiber offset were chosen to be 76 W, 0.3 s, and 50 μm, respectively. We first did the splicing with Taper 1. The loss measured from the SMF to the NC-HCF by the cutback method was 0.37 dB (at 1310 nm), while the loss measured in the reverse direction was 0.67 dB, which included the propagation loss of the 1-meter-long NC-HCF. Figures 5(a1) and 5(a2) show the splice between Taper 1 and the NC-HCF. The total loss of the SMF/NC-HCF/SMF chain was the sum of the two splicing losses and the propagation loss of the 1-meter-long NC-HCF, namely 1.04 dB, where the total splicing loss of the two joints was 0.88 dB. We repeated the splicing with Taper 2 and found that the total splicing loss of the two joints of the SMF/NC-HCF/SMF chain was 1.22 dB, which is slightly larger than the value obtained with Taper 1 and thus verifies our earlier theoretical predication that the use of Taper 1 should lead to a smaller splicing loss than the use of Taper 2.

To observe the cross-sections of the NC-HCF and the taper waist at the joint, we broke the joint by applying a sufficiently large tension to the splice. The well-preserved cladding structure of the NC-HCF at the joint, as shown in Fig. 5(a3), indicates excellent integrity of the fiber during splicing, while the residual marks of the NC-HCF structure on the SMF taper shown in Fig. 5(a4) confirm highly precise axial alignment in the splicing process.
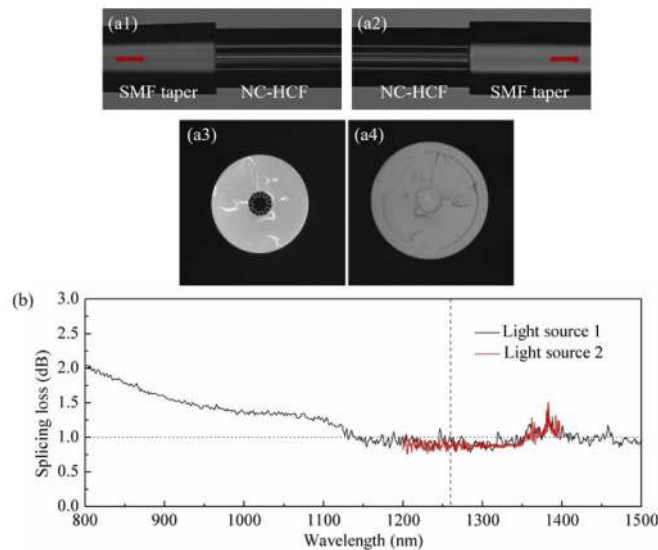
Fig. 5. Side view of (a1) and (a2) SMF/NC-HCF splicing joints and end views of (a3) the NC-HCF and (a4) the SMF reverse taper at a broken joint. The red arrows show the direction of light propagation. (b) Insertion loss of a SMF/NC-HCF/SMF chain measured with two light sources in the wavelength range 800–1500 nm.

The splicing loss of the SMF/NC-HCF/SMF chain in the wavelength range 800–1500 nm (i.e., the insertion loss of the chain with the propagation loss in the NC-HCF subtracted) was measured with two light sources, respectively, and an optical spectrum analyzer. The two light sources were a laser-driven non-coherent source (LDLS, EQ-99X-FC, Energetiq Technology Inc.) (Light source 1) and a superluminescent light-emitting diode (SLED) with a center wavelength of 1310 nm (Light source 2). The measurement results are shown in Fig. 5(b). Firstly, the transmission spectrum was measured using an SMF as a reference, then the SMF was cut in the middle and the two SMF ends were used to splice with the fabricated chain, so the two SMF splice losses were included and our loss measurement was slightly overestimated, however, the normal SMF splice loss is 0.01 dB or less in our experiment, and it can be considered negligible. The loss is smaller than 1.0 dB in the wavelength range 1150–1500 nm, except at the OH^- absorption peak near 1.38 µm. The absorption peak at 1.38 µm was due to the overtone of the OH^- vibration in silica induced by the combustion of the oxy-hydrogen flame with a long TEC duration [30]. As the cutoff wavelength of SMF-28 is ~1260 nm, the relatively large splice loss in the short wavelength range may be caused by the excitation of the higher-order mode of the SMF. From the spectra shown in Fig. 5(b), we find that the total loss of the two splices in the chain at 1310 nm is 0.88 dB, which agrees with the power measurement and, as far as we know, is the lowest fusion splicing loss for a SMF/NC-HCF/SMF chain ever reported.

We finally tested the strengths of the splices formed with the SMF reverse tapers, such as the two joints shown in Figs. 5(a1) and 5(a2). The splices could bear a maximum tension load of ~200 g (average over 5 splices), which is much larger than the maximum tension load (52 g) for splices formed with the 125-µm SMF. We performed another splicing between a SMF reverse taper with a waist diameter of 250 µm and a new NC-HCF sample that also had an overall diameter of 250 µm. The splice could bear a tension load as large as 350 g without breaking. These results confirm the effectiveness of our reverse-tapering process in producing mechanically strong splices by matching the overall diameters of the fibers to be spliced.

4. Conclusion

We have achieved a record-low fusion splicing loss of 0.88 dB for the two joints along a SMF/NC-HCF/SMF chain by using a two-step reverse-tapering method. Our method allows the mode area and the mode-field distribution of a conventional SMF to be precisely controlled to match those of the NC-HCF. We have demonstrated an adiabatic mode-area transformation from 66 μm^2 to 500 μm^2 and the optimal mode area is insensitive to the cleaving position along the waist of the taper. Our method can produce repeatable low-loss splices and is superior to those methods that rely on the use of intermediate bridging elements (such as GRIN fibers). The use of our SMF reverse taper in forming the SMF/NC-HCF fusion splice can increase the mechanical strength of the splice from 52 g to 200 g. As low-loss splicing is a fundamental requirement for optical fiber interconnection and device construction, an application of our splicing method to NC-HCF systems, such as low-latency data transmission [5,31], ultracompact fiber gas cell [10,32,33], HCF resonators and gyroscope [34,35], and HCF quantum technologies [36,37], can immediately improve their performances.

Disclosures. The authors declare no conflicts of interest.

Data availability. Data underlying the results presented in this paper may be available from the corresponding author upon reasonable request.

References

1. F. Poletti, "Nested antiresonant nodeless hollow core fiber," Opt. Express **22**(20), 23807–23828 (2014).
2. B. Debord, A. Amsanpally, M. Chafer, A. Baz, M. Maurel, J. M. Blondy, E. Hugonnot, F. Scol, L. Vincetti, F. Gérôme, and F. Benabid, "Ultralow transmission loss in inhibited-coupling guiding hollow fibers," Optica **4**(2), 209–217 (2017).
3. G. T. Jasion, T. D. Bradley, K. Harrington, H. Sakr, Y. Chen, E. N. Fokoua, I. A. Davidson, A. Taranta, J. R. Hayes, D. J. Richardson, and F. Poletti, "Hollow core NANF with 0.28 dB/km attenuation in the C and L bands," in *Optical Fiber Communication Conference Postdeadline Papers 2020*, (Optical Society of America, 2020), Th4B.4.
4. H. Sakr, K. R. H. Bottrill, N. Taengnoi, N. V. Wheeler, P. Petropoulos, D. J. Richardson, F. Poletti, Y. Hong, T. D. Bradley, G. T. Jasion, J. R. Hayes, H. Kim, I. A. Davidson, E. N. Fokoua, and Y. Chen, "Interband short reach data transmission in ultrawide bandwidth hollow core fiber," J. Lightwave Technol. **38**(1), 159–165 (2020).
5. J. R. Hayes, E. N. Fokoua, M. N. Petrovich, D. J. Richardson, F. Poletti, S. R. Sandoghchi, T. D. Bradley, Z. Liu, R. Slavik, M. A. Gouveia, N. V. Wheeler, G. Jasion, and Y. Chen, "Antiresonant hollow core fiber with an octave spanning bandwidth for short haul data communications," J. Lightwave Technol. **35**(3), 437–442 (2017).
6. M. Ding, Z. Feng, D. Marpaung, X. Zhang, M. Komanec, D. Suslov, D. Dousek, S. Zvanovec, E. R. N. Fokoua, T. D. Bradley, F. Poletti, D. J. Richardson, and R. Slavik, "Optical fiber delay lines in microwave photonics: Sensitivity to temperature and means to reduce it," J. Lightwave Technol. **39**(8), 2311–2318 (2021).
7. C. Yao, L. Xiao, S. Gao, Y. Wang, P. Wang, R. Kan, W. Jin, and W. Ren, "Sub-ppm CO detection in a sub-meter-long hollow-core negative curvature fiber using absorption spectroscopy at 2.3 µm," Sens. Actuators, B **303**, 127238 (2020).
8. R. Yu, Y. Chen, L. Shui, and L. Xiao, "Hollow-core photonic crystal fiber gas sensing," Sensors **20**(10), 2996 (2020).
9. B. Debord, M. Alharbi, L. Vincetti, A. Husakou, C. Fourcade-Dutin, C. Hoenninger, E. Mottay, F. Gerome, and F. Benabid, "Multi-meter fiber-delivery and pulse self-compression of milli-Joule femtosecond laser and fiber-aided laser-micromachining," Opt. Express **22**(9), 10735–10746 (2014).
10. Y. Cui, W. Huang, Z. Wang, M. Wang, Z. Zhou, Z. Li, S. Gao, Y. Wang, and P. Wang, "4.3 µm fiber laser in CO_2-filled hollow-core silica fibers," Optica **6**(8), 951–954 (2019).
11. B. Deng, C. Sima, H. Tan, X. Zhang, Z. Lian, G. Chen, Q. Yu, J. Xu, and D. Liu, "Design of hollow core step-index antiresonant fiber with stepped refractive indices cladding," Front. Optoelectron. 1–6 (2021).
12. F. Amrani, J. H. Osorio, F. Delahaye, F. Giovanardi, L. Vincetti, B. Debord, F. Gerome, and F. Benabid, "Low-loss single-mode hybrid-lattice hollow-core photonic-crystal fibre," Light: Sci. Appl. **10**(1), 7 (2021).
13. W. Huang, Y. Cui, X. Li, Z. Zhou, Z. Li, M. Wang, X. Xi, Z. Chen, and Z. Wang, "Low-loss coupling from single-mode solid-core fibers to anti-resonant hollow-core fibers by fiber tapering technique," Opt. Express **27**(26), 37111–37121 (2019).

14. H. Li, W. Huang, Z. Wang, Z. Zhou, Y. Cui, Z. Li, and X. Xi, "Double-end low-loss coupling of anti-resonant hollow-core fibers with solid-core single-mode fibers by tapering technique," Laser Phys. Lett. **17**(10), 105101 (2020).

15. X. Zheng, B. Debord, L. Vincetti, B. Beaudou, F. Gerome, and F. Benabid, "Fusion splice between tapered inhibited coupling hypocycloid-core Kagome fiber and SMF," Opt. Express **24**(13), 14642–14647 (2016).

16. X. Chen, X. Hu, L. Liao, Y. Xing, G. Chen, L. Yang, J. Peng, H. Li, N. Dai, and J. Li, "High coupling efficiency technology of large core hollow-core fiber with single mode fiber," Opt. Express **27**(23), 33135–33142 (2019).

17. R. Pennetta, S. Xie, F. Lenahan, M. Mridha, D. Novoa, and P. S. J. Russell, "Fresnel-reflection-free self-aligning nanospike interface between a step-index fiber and a hollow-core photonic-crystal-fiber gas cell," Phys. Rev. Appl. **8**(1), 014014 (2017).

18. M. Komanec, D. Suslov, S. Zvanovec, Y. Chen, T. Bradley, S. R. Sandoghchi, E. R. Numkam Fokoua, G. T. Jasion, M. N. Petrovich, F. Poletti, D. J. Richardson, and R. Slavik, "Low-loss and low-back-reflection hollow-core to standard fiber interconnection," IEEE Photon. Technol. Lett. **31**(10), 723–726 (2019).

19. D. Suslov, M. Komanec, S. Zvánovec, T. Bradley, F. Poletti, D. J. Richardson, and R. Slavík, "Highly-efficient and low return-loss coupling of standard and antiresonant hollow-core fibers," in *Frontiers in Optics + Laser Science APS/DLS, OSA Technical Digest* (Optical Society of America, 2019), FW5B.2.

20. D. Suslov, M. Komanec, E. R. Numkam Fokoua, D. Dousek, A. Zhong, S. Zvanovec, T. D. Bradley, F. Poletti, D. J. Richardson, and R. Slavik, "Low loss and high performance interconnection between standard single-mode fiber and antiresonant hollow-core fiber," Sci. Rep. **11**(1), 8799 (2021).

21. T. D. Bradley, J. R. Hayes, Y. Chen, G. T. Jasion, S. R. Sandoghchi, R. Slavik, E. N. Fokoua, S. Bawn, H. Sakr, I. A. Davidson, A. Taranta, J. P. Thomas, M. N. Petrovich, D. J. Richardson, and F. Poletti, "Record low-loss 1.3 dB/km data transmitting antiresonant hollow core fibre," in *2018 European Conference on Optical Communication (ECOC)*, (2018), pp. 1–3.

22. V. Michaud-Belleau, E. Numkam Fokoua, T. D. Bradley, J. R. Hayes, Y. Chen, F. Poletti, D. J. Richardson, J. Genest, and R. Slavík, "Backscattering in antiresonant hollow-core fibers: over 40 dB lower than in standard optical fibers," Optica **8**(2), 216–219 (2021).

23. R. Yu, C. Wang, F. Benabid, K. S. Chiang, and L. Xiao, "Robust mode matching between structurally dissimilar optical fiber waveguides," ACS Photonics **8**(3), 857–863 (2021).

24. K. Z. Aghaie, M. J. Digonnet, and S. Fan, "Optimization of the splice loss between photonic-bandgap fibers and conventional single-mode fibers," Opt. Lett. **35**(12), 1938–1940 (2010).

25. R. Thapa, K. Knabe, K. L. Corwin, and B. R. Washburn, "Arc fusion splicing of hollow-core photonic bandgap fibers for gas-filled fiber cells," Opt. Express **14**(21), 9576–9583 (2006).

26. L. Xiao, M. S. Demokan, W. Jin, Y. Wang, and C.-L. Zhao, "Fusion splicing photonic crystal fibers and conventional single-mode fibers: Microhole collapse effect," J. Lightwave Technol. **25**(11), 3563–3574 (2007).

27. W. D. Pilkey and D. F. Pilkey, *Peterson's stress concentration factors* (John Wiley & Sons, 2008).

28. H. Yamada and H. Hanafusa, "Mode shape convertor produced by the thermal diffusion of different dopants," IEEE Photon. Technol. Lett. **6**(4), 531–533 (1994).

29. S. Gao, Y. Wang, C. Tian, and P. Wang, "Splice loss optimization of a photonic bandgap fiber via a high V-number fiber," IEEE Photon. Technol. Lett. **26**(21), 2134–2137 (2014).

30. J. Stone and C. A. Burrus, "B.S.T.J. brief: reduction of the 1.38-μm water peak in optical fibers by deuterium-hydrogen exchange," Bell Syst. Tech. J. **59**(8), 1541–1548 (1980).

31. Y. Hong, T. D. Bradley, N. Taengnoi, K. R. H. Bottrill, J. R. Hayes, G. T. Jasion, H. C. Mulvad, F. Poletti, P. Petropoulos, and D. J. Richardson, "Comparative investigations between SSMF and hollow-core NANF for transmission in the S + C+L-bands," in *2020 Optical Fiber Communications Conference and Exhibition (OFC)*, (Optical Society of America, 2020), 1–3.

32. T. Billotte, M. Chafer, M. Maurel, F. Amrani, F. Gerome, B. Debord, and F. Benabid, "Contaminant-free end-capped and single-mode acetylene photonic microcell for sub-Doppler spectroscopy," Opt. Lett. **46**(3), 456–459 (2021).

33. Y. Hao, L. Xiao, and F. Benabid, "Optimized design of unsymmetrical gap nodeless hollow core fibers for optofluidic applications," J. Lightwave Technol. **36**(16), 3162–3168 (2018).

34. G. A. Sanders, A. A. Taranta, C. Narayanan, E. Numkam Fokoua, S. Abokhamis Mousavi, L. K. Strandjord, M. Smiciklas, T. D. Bradley, J. Hayes, G. T. Jasion, T. Qiu, W. Williams, F. Poletti, and D. N. Payne, "Hollow-core resonator fiber optic gyroscope using nodeless anti-resonant fiber," Opt. Lett. **46**(1), 46–49 (2021).

35. M. Ding, M. Komanec, D. Suslov, D. Dousek, S. Zvanovec, E. R. N. Fokoua, T. D. Bradley, F. Poletti, D. J. Richardson, and R. Slavik, "Long-length and thermally stable high-finesse Fabry-Perot interferometers made of hollow core optical fiber," J. Lightwave Technol. **38**(8), 2423–2427 (2020).

36. A. Taranta, E. Numkam Fokoua, S. Abokhamis Mousavi, J. R. Hayes, T. D. Bradley, G. T. Jasion, and F. Poletti, "Exceptional polarization purity in antiresonant hollow-core optical fibres," Nat. Photonics **14**(8), 504–510 (2020).

37. X. Chen, W. Ding, Y.-Y. Wang, S.-F. Gao, F. Xu, H. Xu, Y.-F. Hong, Y.-Z. Sun, P. Wang, Y.-Q. Lu, and L. Zhang, "High-fidelity, low-latency polarization quantum state transmissions over a hollow-core conjoined-tube fiber at around 800 nm," Photonics Res. **9**(4), 460–470 (2021).